J. Geogr. Sci. 2019, 29(12): 2101-2121
DOI: https://doi.org/10.1007/s11442-019-1707-x

Moisture sources of the Alashan Sand Seas in western Inner Mongolia, China during the Last Glacial Maximum and mid-Holocene: Interpretation from modern analogues, paleoclimatic simulations and geological records

FENG Yingying[1], *YANG Xiaoping[2]

1. Key Laboratory of Cenozoic Geology and Environment, Institute of Geology and Geophysics, CAS, Beijing 100029, China;
2. Department of Geography, School of Earth Sciences, Zhejiang University, Hangzhou 310027, China

Abstract: Knowledge of moisture sources is of great significance for understanding climatic change and landscape evolution in desert environments. In this paper, we aim to clarify moisture origins for the Alashan (Alxa) Sand Seas (ALSS) in western Inner Mongolia and their transport pathways during the Last Glacial Maximum (LGM) and the mid-Holocene using modern analogues and paleoclimatic simulations. Precipitation data for the period 1959–2015 from meteorological stations in the study area and wind and specific humidity data from the European Center for Medium-Range Weather Forecasts (ECMWF) daily re-analysis were adopted to determine the moisture sources of summer precipitation in the ALSS. In addition paleoclimate simulations under PMIP3/CMIP5 protocols were used to detect the atmospheric circulation and precipitation at 21 ka BP and 6 ka BP over the ALSS. We also reviewed paleoclimate records from the ALSS to acquire a semi-quantitative reconstruction of the moisture history during the late Pleistocene and Holocene. Our results suggest that the summer monsoon transported water vapor from the Indian Ocean and the South China Sea to the ALSS during July and August, causing increased precipitation. The dominant moisture source was from the southwest monsoon, while the East Asian summer monsoon also partly contributed to precipitation in the ALSS. The increased humidity during the period 8.2–4.2 ka BP in the ALSS, as derived from both climate simulation outputs and sedimentary records, was caused by monsoons according to the outputs of simulations. At 21 ka BP, the moisture sources of the ALSS were greatly associated with the prevailing westerlies.

Keywords: Badain Jaran Desert; Tengger Desert; Ulan Buh Desert; Asian summer monsoon; westerlies; paleoclimate

Received: 2019-01-26 **Accepted:** 2019-09-09
Foundation: National Natural Science Foundation of China, No.41430532, No.41672182
Author: Feng Yingying (1994–), specialized in palaeoclimatic simulations.
*Corresponding author: Yang Xiaoping (1964–), Professor, specialized in geomorphology and environmental changes.
E-mail: xpyang@zju.edu.cn

1 Introduction

Large-scale atmospheric circulation plays a vital role in the climate of a region, affecting characteristics such as rainfall by transporting moisture from outside areas, particularly adjacent oceans (Ziv *et al*., 2006; Hastenrath, 2007; Lennard and Hegerl, 2014). Hence, understanding the circulation regime is of central importance for exploring the mechanisms of past climate changes. For understanding climatic change and landscape evolution in desert environments, clarifying moisture sources and their transport pathways is particularly significant.

The Alashan Sand Seas (ALSS) is located in the arid areas of Inner Mongolia, China. Previous studies have shown evidence for the occurrence of long-lasting and extensive paleolakes in the ALSS, a region currently covered primarily by sand dunes (Zhang *et al*., 2001; Yang *et al*., 2003; Chen *et al*., 2014a). Some researchers have reported that the humid periods represented by paleolakes were probably related to Asian summer monsoon intrusions (Yang *et al*., 2003; Yang and Williams, 2003; Zhao *et al*., 2012; Chen *et al*., 2014b), while other studies have excluded the ALSS from monsoon-influenced regions (Wu *et al*., 2012; Wang and Feng, 2013). Modern climate analysis has indicated that the ALSS region is neither a typical monsoon region (Chen *et al*., 2018a) nor in a core westerlies-dominated regime (Huang *et al*., 2015). The ALSS is likely in a transition zone between the monsoon and westerlies-dominated regions (Wang *et al*., 2017).

To clarify the mechanisms triggering climate variations in the ALSS, it is necessary to first determine which circulation pattern enables high precipitation in this region. Here, we examined precipitation data for the period from 1959 to 2015 from meteorological stations and wind and specific humidity data from the European Center for Medium-Range Weather Forecasts (ECMWF) daily reanalysis to determine the moisture sources of rainfall in the ALSS. In addition, we used PMIP3 paleoclimate simulations at 21 ka BP and 6 ka BP to detect the atmospheric circulation pattern and water vapor level over the ALSS at the LGM and mid-Holocene, respectively. We reviewed the climate records from the ALSS region to acquire a semi-quantitative reconstruction of the moisture history during the late Pleistocene and Holocene. Based on these results, we further analyzed the mechanism for humid/arid conditions in the ALSS.

2 Geological and physiographical settings

The Alashan (Alxa) Plateau is located in western Inner Mongolia, China (39°N–42°N, 100°E– 107°E), and has an area of ca. 300,000 km^2 (Figure 1). Tectonically, this region is in accordance with the Alashan Terrane (Yuan and Yang, 2015). In this plateau, there are small mountain ranges higher than 2000 m and some tectonic depressions between these ranges (Li *et al*., 1982). The Alashan Plateau is characterized by a continental climate, with extremely hot summers and cold winters. The mean annual temperature is 7–8℃, and the daily maximum can reach 37–41℃ in summer and -37–-30℃ in winter. Rainfall occurs primarily in July and August, with an average annual precipitation ranging from 45 mm to 215 mm, decreasing from east to west. The main landscapes are the gravel plains of the Alashan Gobi and sandy areas known as the Badain Jaran, Tengger, and Ulan Buh Sand Seas. The Badain Jaran Sand Sea is the second largest sand sea in China and covers an area of 49,000 km^2. The mean annual evaporation has recently been reported as approximately 1040 mm from

the lake surface and approximately 100 mm from the land surfaces in the southeastern part of the sand sea (Yang *et al*., 2010). There are more than 100 permanent lakes between dunes with different sizes, and most of these lakes have a high salinity (Yang and Williams, 2003). The Tengger Sand Sea, situated in the southeastern part of the Alashan Plateau, covers an area of 47,350 km^2. Field investigations and laboratory analyses have shown that during the late Pleistocene, paleolakes covered an area of more than 20,000 km^2, which is more than half the area of the Tengger Sand Sea (Zhang *et al*., 2004). The Ulan Buh Sand Sea is located in the northeast of the Alashan Plateau and covers an area of approximately 11,000 km^2. The surface morphology consists of active, semi-fixed and fixed dunes (Zhu *et al*., 1980).

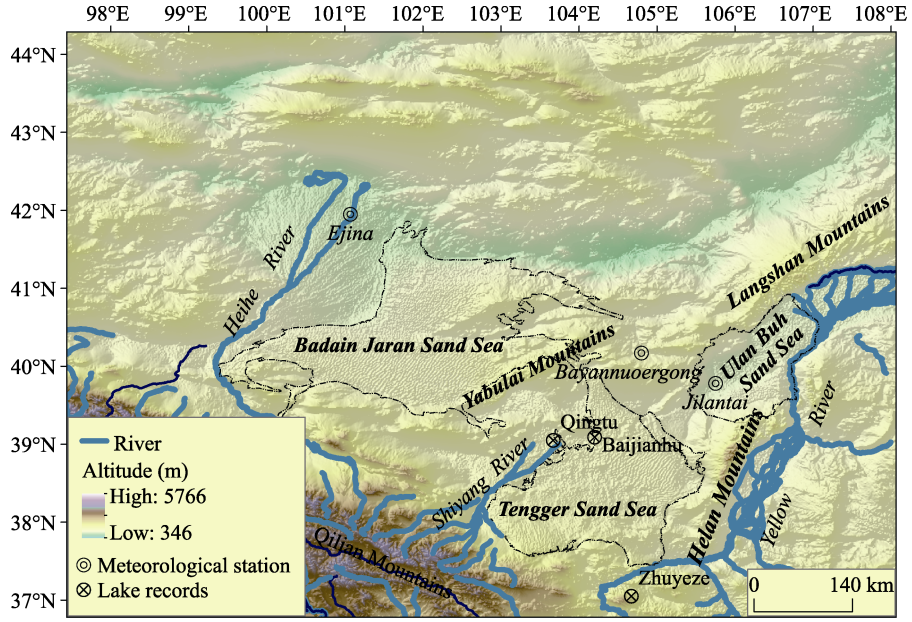

Figure 1 Overview of the Alashan Sand Sea (Badain Jaran Sand Sea, Tengger Sand Sea, Ulan Buh Sand Sea) with the locations of the meteorological stations and main lake record sites referenced in this paper.

3 Methods

3.1 Modern climate analogues

To examine the modern precipitation in the ALSS, precipitation data covering the period 1959–2015 from four meteorological stations, Minqin (38.63°N, 103.08°E), Bayannuoergong (40.17°N, 104.8°E), Jilantai (39.78°N, 105.75°E), and Ejina (41.95°N, 101.07°E), were adopted (Figure 1). The precipitation grades were determined according to the precipitation intensity level standard (Table 1). The ECMWF daily reanalysis data (https://www.ecmwf.int) spanning the period 1958–2016 were adopted to analyze the circulation patterns related to precipitation in the ALSS. Specifically, the ERA-40 dataset for the period 1958–1978 and the ERA-Interim dataset for the period 1979–2016 were used in this study. These are global atmospheric reanalysis products with 4-dimensional variations. ERA-40 has 60 levels in the vertical and approximately uniform 125 km spacing in the horizontal, and the spatial resolution of the ERA-Interim product is approximately 80 km, with 60 ver-

tical levels from the surface up to 0.1 hPa. The variables used for this analysis included the zonal wind, meridional wind, specific humidity, and geopotential height. The water vapor flux was calculated as follows (Trenberth, 1991):

$$Q_u = -\frac{1}{g} qU \tag{1}$$

$$Q_v = -\frac{1}{g} qV \tag{2}$$

where U, V and q represent the zonal wind (m/s), meridional wind (m/s) and specific humidity (kg/kg) of a specific pressure level, respectively, g (m/s^2) is the gravitational acceleration, and Q_u and Q_v are the water vapor fluxes in the zonal and meridional directions, respectively (kg/(m*s)).

In addition, the water vapor sources of precipitation in the ALSS were analyzed using the HYSPLIT-4 model, i.e., Hybrid Single-Particle Lagrangian Integrated Trajectory model (HYSPLIT) of the American National Oceanic and Atmospheric Administration (NOAA) Air Resources Laboratory (ARL). This study used the HYSPLIT back-trajectory analysis, which is a common application of the HYSPLIT model to determine the origins of air masses and establish source-receptor relationships (Fleming *et al*., 2012).

Table 1 Standard precipitation intensity levels (part of inland regions)*

	Light rain	Moderate rain	Heavy rain	Rainstorm
24 h Precipitation	0.1–9.9 mm	10.0–24.9 mm	25.0–49.9 mm	50.0–99.9 mm

*Issued by the China Meteorological Administration (http://www.gov.cn/ztzl/2008tffy/content_1113935.htm).

3.2 Climate simulation

To analyze the precipitation and atmospheric circulation during the LGM and mid-Holocene, transient simulations of five climate models under the latest PMIP3/CMIP5 protocol were used (Table 2). The PMIP3 is the latest Paleoclimate Modelling Intercomparison Project, which is intended to provide an efficient mechanism for coordinating paleoclimate modeling activities, and its protocol includes generally higher horizontal resolutions than the former PMIP1/2 models. The boundary conditions for the LGM and mid-Holocene experiments included changes in the Earth's orbital parameters (Berger, 1978), aerosol concentrations, vegetation, ice sheet extent, topography, and land-sea mask. The Earth's orbital parameters and trace gas concentrations are listed in Table 3. The vegetation was fixed at the pre-industrial state in the AOGCMs and was simulated with dynamic vegetation models in the AOVGCM models. The ice sheet was a blended product obtained by averaging three different ice sheet reconstructions: ICE-6G v2.0, MOCA and ANU. More details about the models and experiments are provided in Taylor *et al*. (2012) and are available online at http://pmip3.lsce.ipsl.fr/. Variables used in this paper included u-wind (m/s), v-wind (m/s), specific humidity (kg/kg), precipitation (mm), and geopotential height (gpm). In addition, the circulation and precipitation outputs for the pre-industrial (PI) control experiment of the five climate models were used for comparing models and different periods.

3.3 Proxy records

To obtain the moisture evolution history in the ALSS region, we reviewed the climate records

Table 2 Basic information of the five climate models within PMIP3 used for the LGM and mid-Holocene experiments in this study

Model	Model type	Atmospheric resolution	Length of run analyzed (year)
CCSM4	AOGCM	1.25° ′ ~0.9°, L26	301
FGOALS-g2	AOVGCM	~2.8° ′ 3–6°, L26	100
CNRM-CM5	AOGCM	~1.4° ′ 1.4°, L31	200
MPI-ESM-P	AOGCM	1.875° ′ ~1.9°, L47	100
MRI-CGCM3	AOGCM	1.125° ′ ~1.1°, L48	100

Note: AOGCM represents coupled atmosphere-ocean general circulation model; AOVGCM represents atmosphere-ocean-vegetation general circulation model.

Table 3 Boundary conditions of orbital parameters and trace gas concentrations in the climate simulations for the LGM and mid-Holocene

	Eccentricity	Obliquity (°)	Precession (ω−180°)	CO_2 (ppm)	CH_4 (ppb)	N_2O (ppb)
LGM	0.018994	22.949	114.42	185	350	200
Mid-Holocene	0.018682	24.105	0.87	280	650	270

in this area to acquire a semi-quantitative reconstruction during the late Pleistocene and Holocene. Climate records from the central sand sea are rare due to the discontinuity of sediments and difficulty of sampling (Tables 4 and 5). To ensure sufficient data quality, all climate records included in our analyses should meet the following criteria:

(1) The roxies should indicate moisture changes, excluding the possibility of changes in local hydrology.

(2) The sequences should be established through a reliable chronology, and the recorded Holocene period should have at least four dating control points.

(3) The sequences should have sufficient resolution (<200 years for the Holocene period).

This paper synthesized 15 records in the ALSS, including lacustrine deposits, former shorelines, and cemented plant roots. For the Holocene period, we transformed the moisture signals from separate studies to a moisture index on a five-point scale (–2, –1, 0, +1, +2). The lowest value (–2) indicated the most arid intervals for each site, while the maximum value (+2) indicated the most humid periods. (0) indicated climate conditions of intermediate stage.

Table 4 List of proxy record sites from the ALSS in the late Pleistocene

Site No.	Site name	Lat. (°N)	Lon. (°E)	Proxy type	Dating method	Number of dates	References
1	Jilantai	39.74	105.70	Pollen, grain size	OSL	4	Fan *et al*. (2017)
2	Tengger	39.15	104.16	Lacustrine terraces	^{14}C	14	Zhang *et al*. (2004)
3	Southeastern margin of Tengger	37.34	105.23	Grain size, Carbonate content. Elemental composition	OSL	4	Qiang *et al*. (2010)
4	Southeast of Badain Jaran	–	–	Aeolian deposits	OSL	26	Fan *et al*. (2016)

Table 5 List of proxy record sites from the ALSS in the Holocene

Site No.	Site name	Lat. (°N)	Lon. (°E)	Proxy type	Dating method	Number of dates	References
1	Badain Jaran	–	–	Lacustrine deposits, Aeolian deposits	^{14}C,TL	5	Yang and Williams (2003)
2	Badain Jaran	–	–	Shorelines	^{14}C	9	Yang *et al*. (2010)
3	Badain Jaran	–	–	Lacustrine deposits, Aeolian deposits, Calcareous cementation layers, cemented plant roots	^{14}C,TL	7	Yang *et al*. (2003)
4	Huahai	40.43	98.07	Grain size, C/N, Carbonate, TOC	^{14}C	17	Wang *et al*. (2013)
5	Tengger	39.15	104.16	Lacustrine terraces	^{14}C	14	Zhang *et al*. (2004)
6	Zhuyeze	37.05	104.67	Grain size, pollen, TOC, T/N	^{14}C	13	Li *et al*. (2008)
7	Baijian Hu	–	–	Shorelines	OSL	25	Long *et al*. (2012)
8	Qingtu Hu	39.05	103.67	Grain size, carbonate, TOC, C/N, δ^{13}C	^{14}C,OSL	16	Long *et al*. (2010)
9	Qingtu Hu	39.07	103.61	Pollen	^{14}C	5	Zhao *et al*. (2008)
10	Ulan Buh	39.77 39.86	105.76 106.39	GPR reflecting, Grain size	OSL	6	Fan *et al*. (2010)
11	Ulan Buh	–	–	Grain size, Loss on ignition, Pollen analysis	OSL	14	Chen *et al*. (2014)
12	Ulan Buh	–	–	Grain size, elevation	OSL	19	Zhao *et al*. (2012)
13	Alashan Sand Sea	–	–	Calcareous root tubes	^{14}C	34	(Li *et al*., 2015a, Li *et al*., 2015b)

4 Results

4.1 Modern moisture sources

The remote moisture source of each moderate rain, heavy rain, and rainstorm (precipitation $\geqslant$ 10 mm during 24 hours) event passing over more than two meteorological stations from 1959 to 2015 in the ALSS was back-tracked. The requirement of covering more than two of the four meteorological stations in the ALSS region aims to exclude non-regional precipitation events. In addition, maximum precipitation $\geqslant$ 10 mm during 24 hours was selected to exclude weak precipitation events that would not significantly improve the effective humidity in the ALSS region. In total, 47 rainfall events met the above conditions and were thus studied (Table 6). The geopotential height and water vapor flux of two typical rainfall events are shown in Figure 2. The results suggest that the dominant precipitation mass source of the ALSS was from the broad high-latitude region from Europe to Siberia (71%) and was carried by mid-level westerly winds. The second source was from the southwestern area over the Indian Ocean via the South China Sea (17.3%) and was transported by southwesterly

Table 6 Details of 47 precipitation events during the period 1959–2015 that affected more than two meteorological stations in the ALSS region with maximum daily precipitation exceeding 10 mm.

No	Start date	Duration (days)	Number of station	Precipitation (min)	Precipitation (max)	Moisture source
1	1958-08-01	1	2	11.4	25.7	Westerlies
2	1958-08-07	1	2	33.2	41.3	Westerlies
3	1960-07-19	3	2	14.5	17	Westerlies
4	1961-07-31	2	2	12	40.4	Westerlies
5	1961-08-06	2	2	26.6	36.5	Westerlies
6	1963-07-20	2	2	14.6	29.9	Westerlies
7	1969-06-15	2	2	11	14	Westerlies
8	1969-08-09	1	2	13.5	14.2	Westerlies
9	1970-08-01	1	2	14	18	Westerlies
10	1970-08-17	2	2	24.2	33.1	Monsoon
11	**1973-08-10**	**4**	**3**	**11.9**	**32.9**	**Monsoon**
12	1973-08-15	2	2	10.2	36.6	Westerlies
13	**1974-07-28**	**3**	**4**	**10.6**	**42.1**	**Monsoon**
14	1977-07-28	1	3	11.6	44	Westerlies
15	**1977-08-19**	**2**	**3**	**10.2**	**34.2**	**Westerlies**
16	1978-07-27	3	4	10.9	20.3	Westerlies
17	1979-07-01	2	2	10.9	15	Westerlies
18	**1979-07-18**	**4**	**3**	**13**	**32.4**	**Monsoon**
19	1979-08-06	2	2	26.5	27.9	Monsoon
20	1980-08-01	2	2	10.3	13.5	Monsoon
21	1981-07-02	1	3	14.6	23.8	Westerlies
22	1983-08-13	1	2	20.1	20.9	Monsoon
23	1984-06-13	1	2	13.8	19.3	Westerlies
24	1993-07-20	2	2	28.4	31.2	Westerlies
25	1993-08-10	1	2	13.4	17.7	Westerlies
26	1993-08-29	1	2	14.2	21	Westerlies
27	1994-07-07	1	2	20.2	28.7	Westerlies
28	1994-08-12	1	3	14	18	Westerlies
29	1995-08-10	1	2	10.4	14.8	Westerlies
30	1995-08-15	2	2	18	24.1	Westerlies
31	1996-07-27	3	3	13.1	24	Westerlies
32	1997-07-30	1	2	12.4	17.6	Monsoon
33	1998-06-11	1	3	10.3	44	Monsoon
34	1999-07-06	1	2	11.1	20.5	Westerlies
35	2000-08-07	1	2	11.9	19.1	Westerlies
36	**2002-06-07**	**2**	**3**	**18.9**	**31.2**	**Monsoon**
37	2002-06-21	1	2	21.3	23	Westerlies
38	2003-06-25	1	3	14.1	24.8	Westerlies
39	2003-08-29	1	2	11.4	14.3	Westerlies

(*To be continued on the next page*)

(*Continued*)

No	Start date	Duration (days)	Number of station	Precipitation (min)	Precipitation (max)	Moisture source
40	2006-08-17	2	2	13.5	26	Monsoon
41	**2008-07-28**	**2**	**3**	**12.1**	**33.2**	**Monsoon**
42	2009-08-18	1	3	13.3	26.5	Westerlies
43	2012-06-27	1	2	16.5	34.6	Westerlies
44	2012-07-29	2	2	14.5	33.1	Monsoon
45	2016-06-02	1	2	12.2	18.3	Westerlies
46	2016-07-10	1	2	13	16.3	Westerlies
47	2016-08-13	1	2	14.5	22.6	Monsoon

Note: Start date refers to the first day of a precipitation event. Precipitation (min) is the minimum daily precipitation (mm) of all meteorological stations observing precipitation. Precipitation (max) is the maximum daily precipitation (mm) of all meteorological stations observing precipitation. Number of stations is the number of meteorological stations that recorded a rainfall event. The statistics include four meteorological stations: Minqin (38.63°N, 103.08°E), Bayannuoergong (40.17°N, 104.8°E), Jilantai (39.78°N, 105.75°E) and Ejina (41.95°N, 101.07°E). The bold font indicates "regional severe precipitation events".

monsoon winds. The third source was a southeastern source from the western North Pacific (11.7%), transported by the trade winds of the southern flank flow of the western North Pacific Subtropical High.

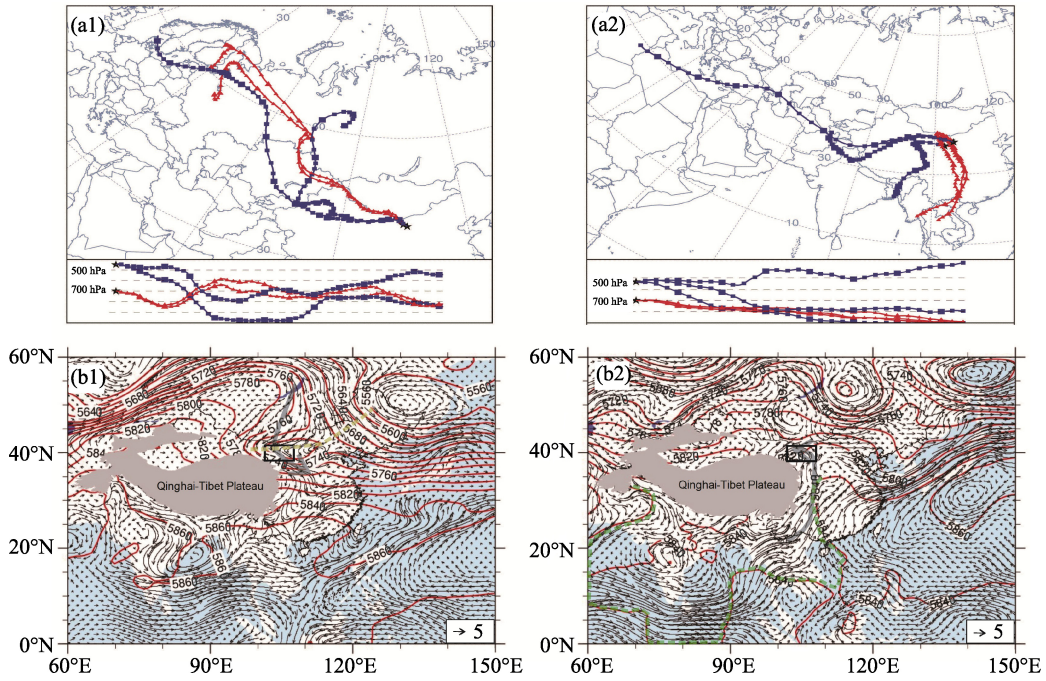

Figure 2 Backward water vapor trajectories before rainfall in the ALSS (a1, a2) and the atmospheric circulation (500 hPa geopotential height (gpm) and water vapor flux (g/(m*s)) at 700 hPa) (b1, b2) of two typical rainfall events. a1, b1: Rainfall event on June 15, 1969, where the westerlies transported the moisture for precipitation in ALSS. a2, b2: Rainfall event on July 30, 1974, where the summer monsoon transported the moisture. The blank rectangle refers to the ALSS region, the yellow dashed line is the westerly trough, and the green dashed line circles the trough region between the Arabian Peninsula High and the West Pacific Subtropical High.

Furthermore, we defined rainfall events occurring at more than three meteorological stations in the ALSS region with maximum precipitation ⩾ 25 mm in 24 hours and lasting for more than two days as "regional severe precipitation events". The results suggested that, in most regional sever precipitation events, the moisture was transported by the summer monsoon (Figure 3).

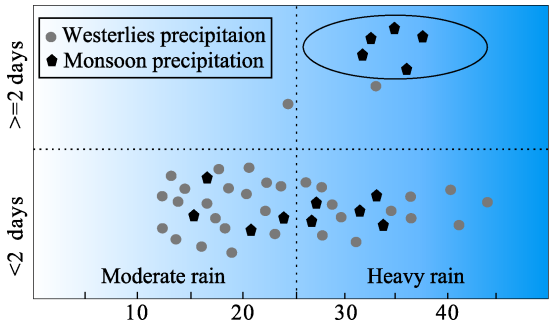

Figure 3 Moisture source statistics for the following rain types: moderate rain, and heavy rain refer to rainfall for 2 or fewer days, and rainfall for more than 2 days, respectively. Only rainfall events covering more than two of the four meteorological stations were analyzed.

During the majority of regional severe precipitation events, the trough between the Arabian Peninsula High and the West Pacific Subtropical High (green dashed line in Figure 2) was deepened, favoring the northward transport of the southwest air current between the two high pressures. Furthermore, the westerly trough in the region of Mongolia (100°E–110°E) (yellow dashed line in Figure 2), which would restrain the northward flow of southern air in southwestern China, became weaker or even nearly disappeared.

4.2 Simulated paleomoisture sources

For the LGM period, all of the climate models suggest that the water vapor source of the ALSS was the high-latitude region from Europe to Siberia, and the moisture was transported by the westerly wind (Figures 6–10). The westerly winds in the LGM experiments were stronger and more southward in the 100–110°E region than those in the PI experiments (Figure 4). In addition, the westerly trough in Mongolia was deepened and stretched to a more southern latitude, favoring the southward propagation of the westerlies.

In the mid-Holocene, CCSM4, FGOALS-g2, CNRM-CM5, and MPI-ESM-P suggest that the dominant precipitation masses of the ALSS originated from the southwestern source over the Indian Ocean via the South China Sea and were carried by southwesterly monsoons. Differently, the MRI-CGCM3 model indicates that westerlies in the 100–110°E region turned southward to 33°N and controlled the ALSS region. However, the PI control experiment suggests that the westerlies in the MRI-CGCM3 climate model were further south (30°N) in the 100°–110°E region (Figure 4), which is not in accordance with the other four models. Thus, the MRI-CGCM3 result that the summer monsoon failed to control the ALSS region in the mid-Holocene may due to this model's inaccuracy in predicting the water vapor flux. All of the models suggest that the westerly trough over the region of Mongolia had a more northern location than in the PI control experiments, which also favored the northward movement of the southern current.

To determine the difference in moisture transport between the mid-Holocene and LGM period, we calculated the difference in the water vapor flux between the mid-Holocene and LGM (Figure 11). The results suggest that except for the MRI-CGCM3 model, all models indicate a southerly wind over the ALSS region in the difference calculation. In other words, in the summer of the mid-Holocene, the southerly wind, i.e., summer monsoon, was stronger than during the LGM period.

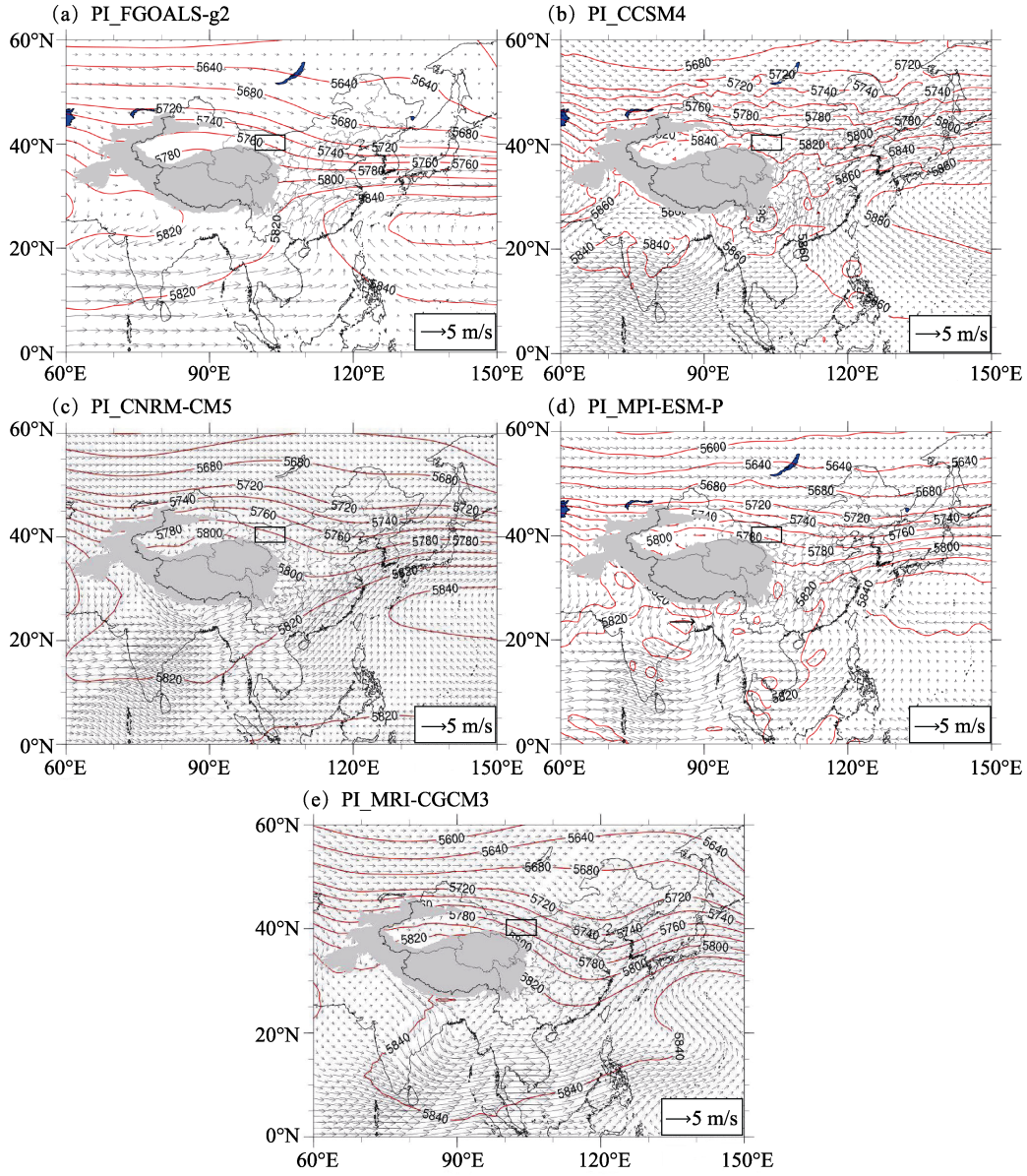

Figure 4 The simulation outputs for the water vapor flux at 700 hPa (g/(m*s)) and 500 hPa geopotential height (gpm) for the PI control experiment. (a): FGOALS-g2; (b): CCSM4; (c): CNRM-CM5; (d): MPI-ESM-P; and (e): MRI-CGCM3. The blank rectangle refers to the ALSS region.

The average annual precipitation amounts in the LGM, mid-Holocene and PI period of the five climate models were calculated (Figure 5). The FGOALS-g2 model indicates that the average annual precipitation of the ALSS region in the mid-Holocene experiment was 200–300 mm, while in the LGM experiment it was 50–200 mm. The CCSM4 model indicates similar annual precipitation amounts, i.e., 100–300 mm in the mid-Holocene and 50–200 mm in the LGM. CNRM-CM5 indicates a mid-Holocene average annual precipitation of 100–200 mm, with 50–200 mm during the LGM. For the MPI-ESM-P model, the average annual precipitation in the mid-Holocene period was 100–300 mm, while that in the

LGM period was 50–200 mm. The mean annual precipitation in the MRI-CGCM3 model was 50–200 mm in the mid-Holocene and 50–100 mm in the LGM.

Overall, in the mid-Holocene, the ALSS exhibited higher precipitation than in the PI and LGM periods. Four of the five studied climate models indicate that the summer monsoon arrived in the ALSS in the mid-Holocene, while the westerlies of this period had a more northward location than during the PI and LGM periods. From the water vapor flux map (Figures 6–10), we found that the mid-Holocene period was characterized by a strong moisture transport belt that started in the Arabian Sea and the Bay of Bengal and passed through southwestern China, eastern China, and northeastern China. In the LGM period, this moisture transport belt remained only in the southern region.

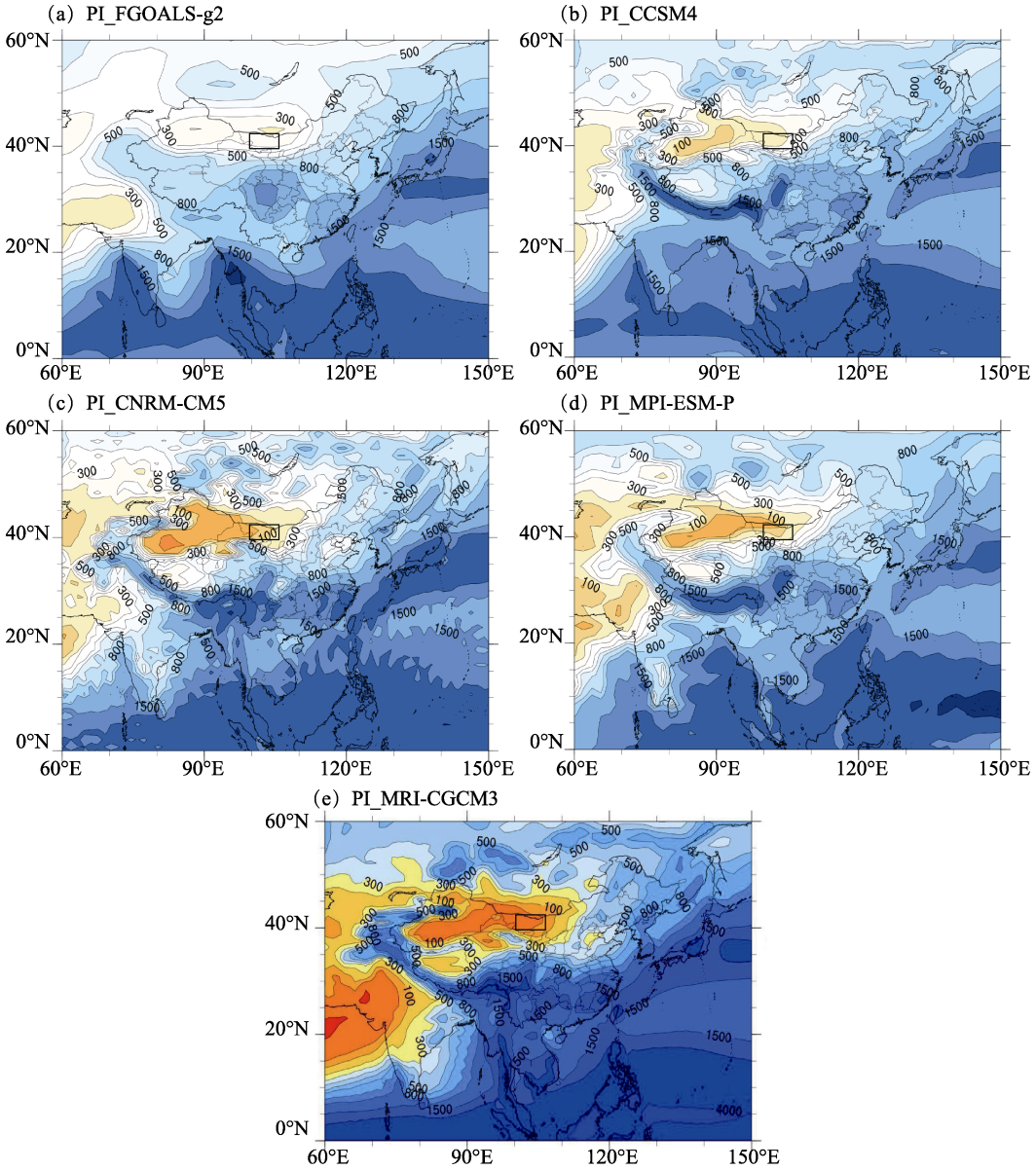

Figure 5 The simulation outputs for annual precipitation (mm) in the PI control experiment. (a): FGOALS-g2; (b): CCSM4; (c): CNRM-CM5; (d): MPI-ESM-P; and (e): MRI-CGCM3. The blank rectangle refers to the ALSS region.

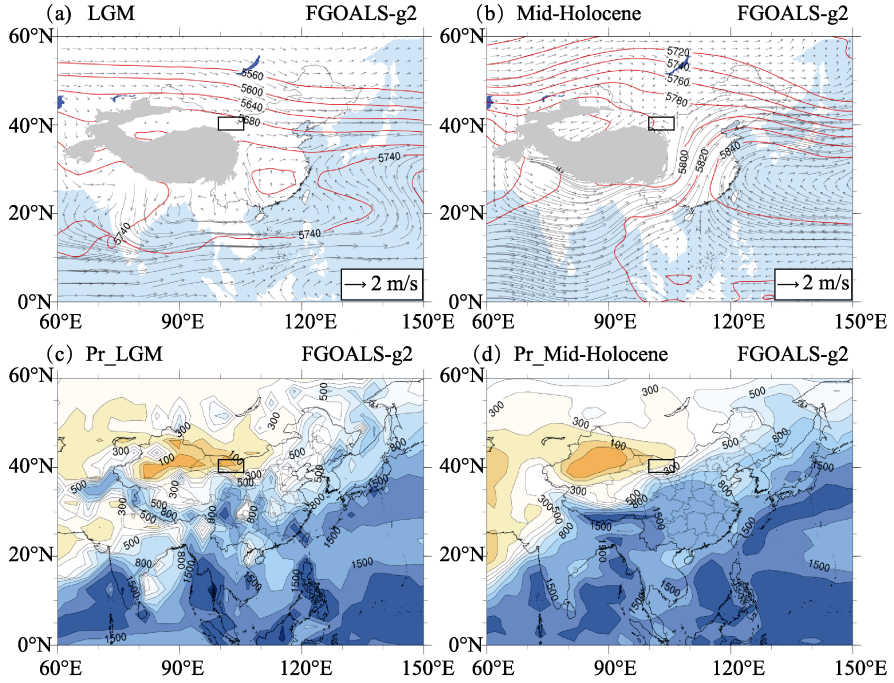

Figure 6 The FGOALS-g2 simulation outputs for the LGM and mid-Holocene. (a–b): atmospheric circulation (water vapor flux at 700 hPa (g/(m*s)) and 500 hPa geopotential height (gpm)); (c–d): annual precipitation (mm). The blank rectangle refers to the ALSS region.

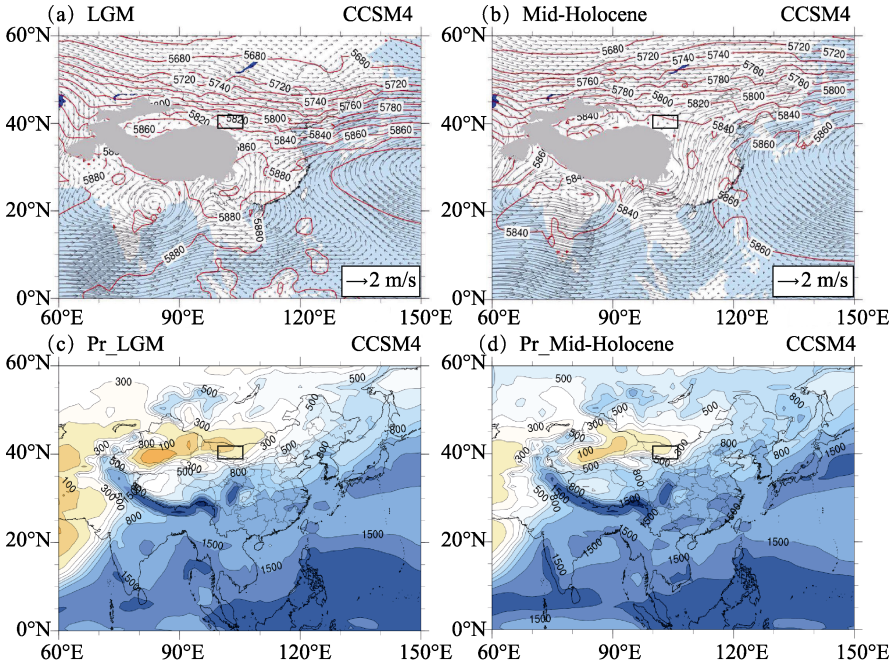

Figure 7 The CCSM4 simulation outputs for the LGM and mid-Holocene. (a–b): atmospheric circulation (water vapor flux at 700 hPa g/(m*s)) and 500 hPa geopotential height (gpm)); (c–d): annual precipitation (mm). The blank rectangle refers to the ALSS region.

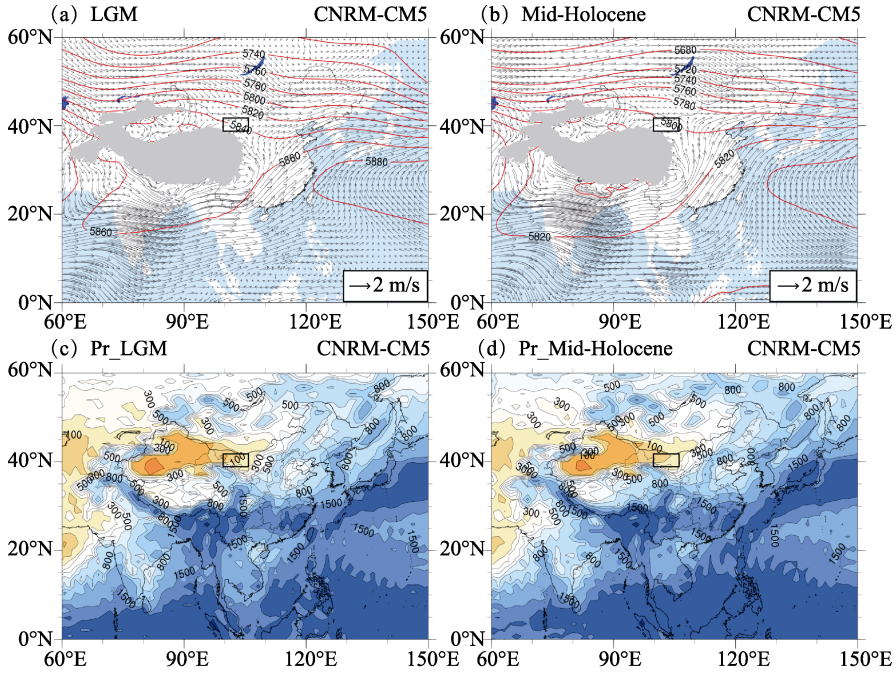

Figure 8 The CM5 simulation outputs for the LGM and mid-Holocene. (a–b): atmospheric circulation (water vapor flux at 700 hPa (g/(m*s)) and 500 hPa geopotential height (gpm)); (c–d): annual precipitation (mm). The blank rectangle refers to the ALSS region.

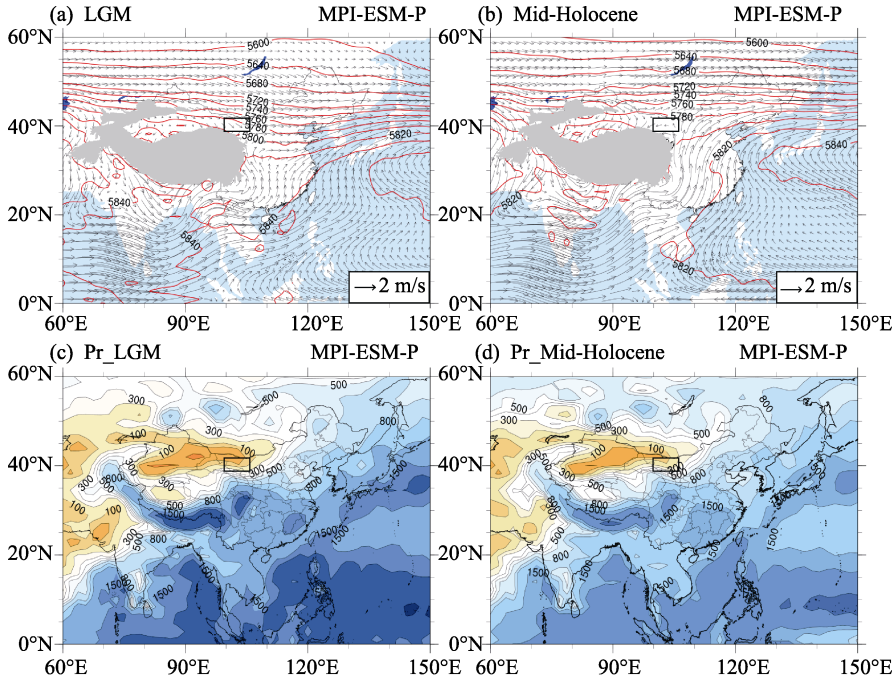

Figure 9 The MPI-ESM-P simulation outputs for the LGM and mid-Holocene. (a–b): atmospheric circulation (water vapor flux at 700 hPa (g/(m*s)) and 500 hPa geopotential height (gpm)); (c–d): annual precipitation (mm). The blank rectangle refers to the ALSS region.

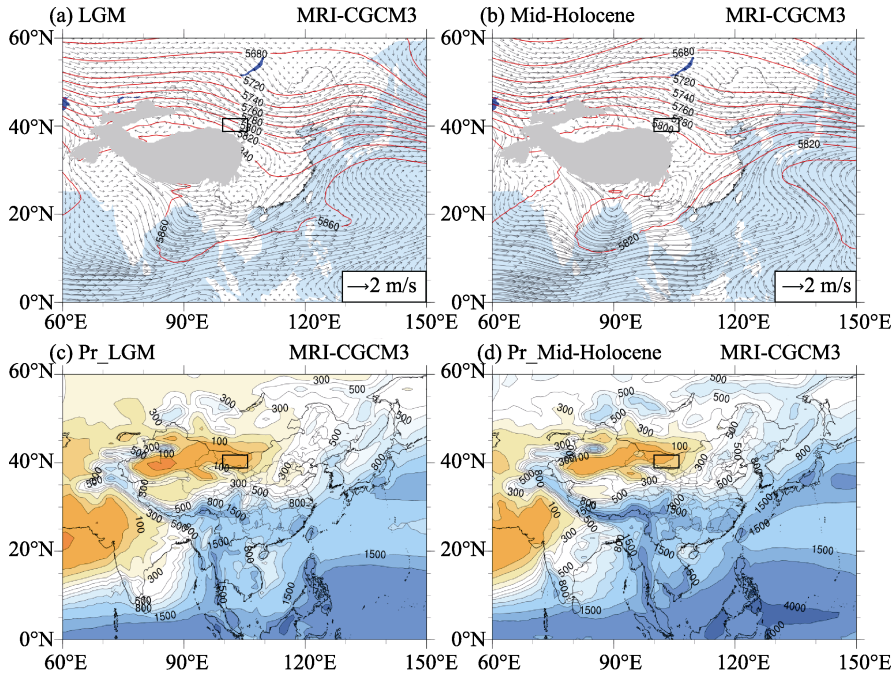

Figure 10 The MRI-CGCM3 simulation outputs for the LGM and mid-Holocene. (a–b): atmospheric circulation (water vapor flux at 700 hPa (g/(m*s)) and 500 hPa geopotential height (gpm)); (c–d): annual precipitation (mm). The blank rectangle refers to the ALSS region.

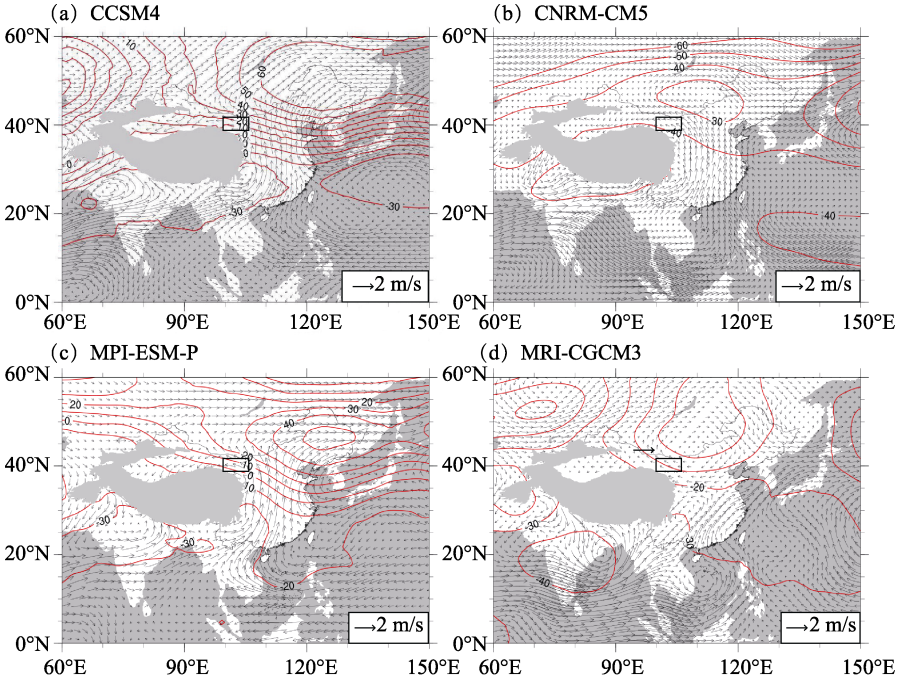

Figure 11 The difference in the atmospheric circulation between the mid-Holocene and LGM (water vapor flux at 700 hPa (g/(m*s)) and 500 hPa geopotential height (gpm)). (a): CCSM4; (b): CNRM-CM5; (c): MPI-ESM-P; and (d): MRI-CGCM3. The blank rectangle refers to the ALSS region.

4.3 Moisture history of the ALSS interpreted from a synthesis of published records

4.3.1 The late Pleistocene

Field investigations and the optically stimulated luminescence (OSL) dating of 14 profiles suggest that the Badain Jararn's expansion was initiated at 20 ka (Fan *et al*., 2016). A high lake level existed in the Tengger Sand Sea during the period 39–22 ka BP (Zhang *et al*., 2004), and a sharp increase in wind speeds and dry conditions occurred in the subsequent period (19.1–11.4 ka BP) (Qiang *et al*., 2010). Two drill cores obtained from the Jilantai sub-depression and the neighboring Dengkou sub-uplift show that the Jilantai sub-depression had been continuously covered by lakes since 85 ka BP, while the Dengkou sub-uplift was covered by lakes during the periods 80–74 ka, 50–44 ka, 32.5–27.5 ka, and <13 ka and was covered by aeolian deposits during the periods 44–32.5 ka and 27.5–13 ka (Fan *et al*., 2017). Overall, the ALSS was relatively humid during the period 40–30 ka, after which the climate tended to be dry until 11.4 ka BP (Jin *et al*., 2015).

4.3.2 The Holocene

Only a few climate records are available from the central Badain Jaran Sand Sea because of the discontinuity of the sediments and difficulty of sampling. During the early Holocene, records from the inner sand sea reveal wet conditions (Yang and Williams, 2003). Lake sediments from Huahai also indicate increased moisture in the region during the early Holocene (Wang *et al*., 2012). The moisture maximum of the entire record occurred in the mid-Holocene; during this period, all records uniformly suggest wet conditions (Yang and Williams, 2003; Yang *et al*., 2003; Yang *et al*., 2010; Wang *et al*., 2013). After that, the climate tended to become drier, as recorded by lacustrine and aeolian deposits (Yang and Williams, 2003; Wang *et al*., 2013). Overall, the records from the inner sand sea and the southeastern margin suggest that there were wet conditions in the early to mid-Holocene.

The period in the early Holocene (11.7–8.2 ka BP) is marked by a low moisture availability in the Tengger Sand Sea (Li *et al*., 2008; Zhao *et al*., 2008; Long *et al*., 2010). The Tengger Sand Sea experienced wet conditions in the mid-Holocene (Li *et al*., 2008; Zhao *et al*., 2008; Long *et al*., 2010; Li *et al*., 2015a; 2015b), for which a high lake level was recorded (Zhang *et al*., 2004; Long *et al*., 2012). The period after 5.0 ka BP experienced a return to a lower moisture availability (Li *et al*., 2008; Zhao *et al*., 2008; Long *et al*., 2010; Long *et al*., 2012), although a high lake level was recorded for 3.5 ka BP (Zhang *et al*., 2004).

In the period 8–7 ka BP, the environment was wet and characterized by the formation of numerous interdune ponds throughout the Ulan Buh Sand Sea (Chen *et al*., 2014b), although sand dunes persisted in the southern Ulan Buh Sand Sea (Zhao *et al*., 2012; Chen *et al*., 2014b). After 6.5 ka BP, the paleolake shrank and broke apart (Zhao *et al*., 2012), and the modern Ulan Buh landscape formed. During the last 2000 years, the northern Ulan Buh Sand Sea has been invaded by aeolian sands from the Badain Jaran Sand Sea, and the eastern Ulan Buh area was formed by farming and overgrazing (Fan *et al*., 2010; Zhao *et al*., 2012). Overall, the calculated moisture index suggests a humid period during the period 8.2–4.2 ka in the ALSS region (Figure 12).

5 Discussion

5.1 The mechanism of moisture evolution in the ALSS

Some geological records suggest that the summer monsoon probably intruded into the core

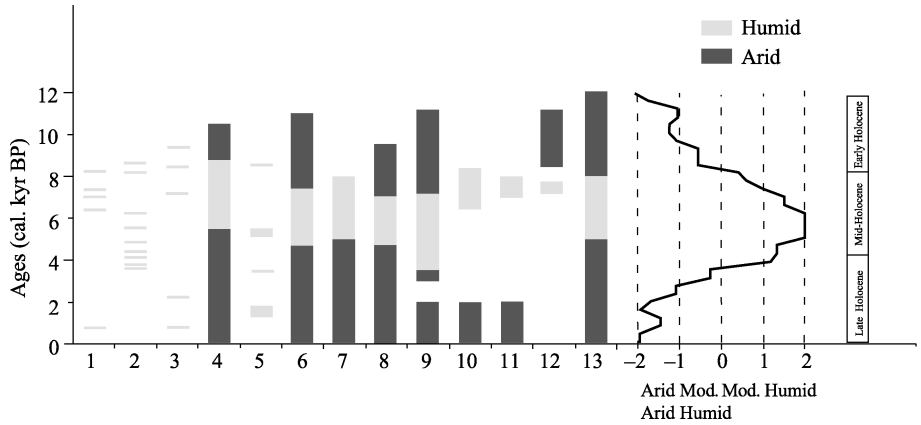

Figure 12 Holocene moisture evolution of the ALSS region in previous studies and our calculated moisture index. –2, –1, 0, +1, and +2 represent the calculated moisture index. –2 indicates the most arid intervals for each site; –1 indicates an arid environment; 0 indicates a climate condition of intermediate stage; 1 indicates a humid environment; and 2 indicates the most humid environment. The locations of sediment sites marked by the numbers 1–13 in this figure are given in Table 5.

area of the ALSS at approximately 8–4 ka BP, bringing abundant moisture (Yang and Williams, 2003), while others exclude the ALSS from the monsoon-influenced region, suggesting this region had an arid environment in the mid-Holocene (Wang and Feng, 2013; Wu *et al*., 2012). However, our study on the modern moisture sources of the ALSS region suggests that during the period 1959–2015, most regional severe precipitation events were related to water vapor transported by the summer monsoon. Because the summer monsoon in the early to mid-Holocene was stronger than the current summer monsoon (Leuschner and Sirocko, 2003; Caley *et al*., 2011), it is possible that the summer monsoon brought moisture to the ALSS at a higher frequency in the mid-Holocene than at present. This hypothesis is supported by the climate simulation results of various models, in which the summer monsoon delivered moisture from the Indian Ocean and South China Sea to the ALSS at 6 ka BP. Accordingly, the annual precipitation in the mid-Holocene was 50–200 mm higher than during the LGM. Although some studies have found that the wet (dry) conditions are sometimes not directly (inversely) proportional to stronger (weaker) water vapor fluxes (Zhang and Jin, 2016), the ALSS region suggests a positive correlation between the water vapor flux and precipitation.

According to the modern climate analogue, westerly winds can also bring effective moisture to the region. However, the amount of precipitation delivered via this mechanism is less than the amount of precipitation during events related to the summer monsoon. Hence, we hypothesize that the dry period of the ALSS was related to a westerly-dominated circulation. The climate simulations also suggest that the westerly circulation dominated in the study area during the LGM.

Previous studies have reported the existence of a period of high lake levels in the ALSS region. Chen *et al*. (2014b) proposed that a possible driving force for mega-lake formation is increased summer monsoon rainfall. Yang *et al*. (2003) proposed that the humid period in the Badain Jaran Sand Sea may imply a periodic change in the intensity of the westerlies and the Asian monsoon. Our simulations demonstrate that summer monsoons can bring moisture into the ALSS and has caused heavy rainfall in the recent geologic history.

5.2 Comparison with paleoclimate proxy records

The results suggest that most moisture from regional severe precipitation events is transported by the southwest monsoon. Thus, we compared the moisture evolution history in the ALSS with that in a typical southwest monsoon region. Because the southwest monsoon is the northeastern branch of the Indian summer monsoon, the evolution of the southwest monsoon should have a close relationship with the Indian summer monsoon. The Indian summer monsoon is formed by the seasonal movement of the planetary wind system, in which southeasterly trade winds cross the equator in summer and turn eastward (Caley *et al*., 2011). Thus, the Indian summer monsoon is highly sensitive to insolation differences, and the monsoon intensity during the Holocene reached its maximum at 11.7–8.2 ka BP (Agnihotri *et al*., 2002; Leuschner and Sirocko, 2003; Herzschuh, 2006). After that period, the monsoon intensity decreased in response to declining summer insolation (Overpeck *et al*., 1996; Fleitmann *et al*., 2007). The evolution of the southwest monsoon in the Holocene was recorded by lake sediments in southwestern China, which is the domain region of the southwest monsoon. The early Holocene was characterized by an effective moisture maximum (Xinghu Lake and Qilu Lake: 12–8 ka BP (Hodell *et al*., 1999); Erhai: 12.9–6.3 ka BP (Ji *et al*., 2005b); and Lugu Lake: 10.3–7.5 ka BP (Zheng *et al*., 2014)), and the effective moisture then decreased gradually. The Tibetan Plateau is also considered to be influenced by the southwest monsoon in summer (Liu *et al*., 2007; Tian *et al*., 2007). High lake levels and favorable vegetation conditions recorded the humid period in the early to mid-Holocene on the Tibetan Plateau (e.g., Qinghai Lake: 11.7–4.2 ^{14}C ka BP (Ji *et al*., 2005a); Ahung Co: 9.0–7.5 ka BP (Morrill *et al*., 2006); Seling Co: 10.0–4.2 ka BP (Gu *et al*., 1993); and Hongyuan peat: 11.2–5.5 ka BP (Hong *et al*., 2003)), and dry climate conditions have occurred since approximately 4.0 ka BP (Sun *et al*., 1993; Hong *et al*., 2003; Ji *et al*., 2005a; Morrill *et al*., 2006).

The East Asian summer monsoon is formed by thermal differences between the land and sea. Lake sediments indicate the lake status in the East Asian summer monsoon region has been stable and consistent with high precipitation levels since approximately 11 ka BP, and the Holocene moisture maxima occurred at ~8–5 ka (Ganhai: 8.0–5.8 ^{14}C ka BP (Zhang *et al*., 2018); Gonghai: 7.8–5.3 ^{14}C ka BP (Chen *et al*., 2018b); Daihai: and 7.9–4.45 cal a BP (Xiao *et al*., 2004)). The current dry climate began at approximately 4 ka BP in the EASM region (Ganhai: 4.3 ka BP (Zhang *et al*., 2018); Gonghai: 3.2 ka BP (Chen *et al*., 2018b); 4.45 ka BP (Xiao *et al*., 2004)). Peat records indicate that the summer monsoon strengthened in the early and mid-Holocene (Dahu swamp: ca. 10–6 ka BP (Zhong *et al*., 2010); Dajiuhu peat: 6.7–4.2 ^{14}C ka BP (Ma *et al*., 2008)) and tended to dry thereafter. Overall, multi-proxy records for the East Asian summer monsoon region yield a generally consistent timing of the Holocene optimum during the mid-Holocene period.

5.3 Relationship between monsoon intensity and ALSS moisture history

The summer monsoon in East Asia consists of three branches. The southwest branch is the extension of the Indian summer monsoon to the East Asian monsoon zone, the middle branch is the cross-equatorial flow between 110°E and 130°E in the Southeast Asia area, and the eastern branch is the southwesterly flow on the western side of the West Pacific Subtropical High (Zhu *et al*., 1986; Liu *et al*., 2004). Based on previous studies, it remains un-

clear which branch transports major part of moisture to the ALSS. Our results indicate that the southwest monsoon is the main source of the summer moisture in the ALSS. The Arabian Sea, the Bay of Bengal, and the South China Sea are the dominant moisture sources for the ALSS. This finding is consistent with studies by Ding *et al*. (2004) and Qian *et al*. (2007), who reported strong moisture transport from the Indian Ocean to the west of 110°E in China. However, the moisture evolution in the ALSS during the Holocene was not completely consistent with that in a typical southwest monsoon region. In fact, in the modern climate analogue, the precipitation in the ALSS is not significantly sensitive to the intensity of the southwest monsoon. Southwestern China is more sensitive than the ALSS, which could explain why the precipitation evolution of southwestern China during the Holocene was consistent with the intensity of the southwestern/Indian monsoon (Li and Zeng, 2002). When the West Pacific Subtropical High extends westward, more precipitation tends to occur in East Asia (Chen and Wu, 1998; Lu, 2001). When the East Asian westerly jet is south (north) of its normal position, the above-normal (below-normal) precipitation tends to occur in East Asia (Liang and Wang, 1998; Lau *et al*., 2000; Lu, 2004). Our study suggests that the favorable circulation conditions for the northward movement of the monsoon to the ALSS occur when the trough between the Arabian Peninsula High and the West Pacific Subtropical High is deep and the Westerly Trough in the Mongolian region is weak. The climate simulations suggest that at 6 ka BP, the circulation met this favorable pattern, which explains why the ALSS received abundant moisture at that time.

In the modern climate analogue, apart from the southeast monsoon source of moisture, the southeastern source of moisture from the western North Pacific via the trade winds on the southern flank flow of the western North Pacific Subtropical High is also responsible for the severe precipitation events in the ALSS. The only period in which both the Southwest and East Asian monsoons were strong was the mid-Holocene. Because the climate simulations of moisture transport patterns reflect an average climate state, it is quite likely that the East Asian monsoon also transported moisture to the ALSS during regional severe precipitation events.

6 Conclusions

Modern moisture transport analogues and paleoclimate simulations suggest that the summer monsoon can transport water vapor from the Indian Ocean and the South China Sea to the ALSS. Although moisture from westerlies can also produce summer rainfall in the ALSS, most regional severe precipitation events are linked to summer monsoon moisture. The dominant moisture transport path follows the southwest monsoon, and the southeastern source from the trade winds on the southern flank of the western North Pacific Subtropical High is also responsible for monsoon precipitation in the ALSS. Paleoclimatic modeling for 21 ka BP and 6 ka BP suggest that the mid-Holocene was characterized by summer monsoon moisture transportation and higher precipitation than the PI period, while in the LGM period, the main moisture source was from the broad high-latitude region extending from Europe to Siberia, carried by mid-level westerly winds. The results of the climate simulations are consistent with the climate records acquired in the ALSS region and demonstrate the different roles of the summer monsoon and westerlies in the paleoclimatic history of the ALSS.

Acknowledgements

We would like to thank the editors and three anonymous reviewers for their constructive comments on earlier draft of this paper.

References

Agnihotri R, Dutta K, Bhushan R *et al*., 2002. Evidence for solar forcing on the Indian monsoon during the last millennium. *Earth and Planetary Science Letters*, 198(3/4): 521–527.

Berger A L, 1978. Long term variations of daily insolation and Quaternary climatic changes. *Journal of the Atmospheric Sciences*, 35(12): 2362–2367.

Caley T, Malaizé B, Revel M *et al*., 2011. Orbital timing of the Indian, East Asian and African boreal monsoons and the concept of a 'global monsoon'. *Quaternary Science Reviews*, 30(25/26): 3705–3715.

Chen F, Chen X, Chen J *et al*., 2014a. Holocene vegetation history, precipitation changes and Indian Summer Monsoon evolution documented from sediments of Xingyun Lake, south-west China. *Journal of Quaternary Science*, 29(7): 661–674.

Chen F, Li G, Zhao H *et al*., 2014b. Landscape evolution of the Ulan Buh Desert in northern China during the late Quaternary. *Quaternary Research*, 81(3): 476–487.

Chen J, Huang W, Jin L *et al*., 2018a. A climatological northern boundary index for the East Asian summer monsoon and its interannual variability. *Science China Earth Sciences*, 61(1): 13–22.

Chen L, Wu R, 1998. Relationship between summer rainbelt patterns in the eastern China and 500 hPa circulation anomalies over the Northern Hemisphere. *Scientia Atmospherica Sinica*, 22(6): 849–857. (in Chinese)

Chen S, Liu J, Xie C *et al*., 2018b. Evolution of integrated lake status since the last deglaciation: A high-resolution sedimentary record from Lake Gonghai, Shanxi, China. *Palaeogeography*, *Palaeoclimatology*, *Palaeoecology*, 496: 175–182.

Ding Y H, Li C Y, Liu Y J, 2004. Overview of the South China Sea monsoon experiment. *Advances in Atmospheric Sciences*, 21(3): 343–360.

Fan Y, Chen F, Fan T *et al*., 2010. Sedimentary documents and optically stimulated luminescence (OSL) dating for formation of the present landform of the northern Ulan Buh Desert, northern China. *Science China Earth Sciences*, 53(11): 1675–1682.

Fan Y, Wang Y, Mou X *et al*., 2017. Environmental status of the Jilantai Basin, North China, on the northwestern margin of the modern Asian summer monsoon domain during Marine Isotope Stage 3. *Journal of Asian Earth Sciences*, 147: 178–192.

Fan Y, Zhang F, Zhang F *et al*., 2016. History and mechanisms for the expansion of the Badain Jaran Desert, northern China, since 20 ka: Geological and luminescence chronological evidence. *The Holocene*, 26(4): 532–548.

Fleitmann D, Burns S J, Mangini A *et al*., 2007. Holocene ITCZ and Indian monsoon dynamics recorded in stalagmites from Oman and Yemen (Socotra). *Quaternary Science Reviews*, 26(1/2): 170–188.

Fleming Z L, Monks P S, Manning A J, 2012. Review: Untangling the influence of air-mass history in interpreting observed atmospheric composition. *Atmospheric Research*, 104/105: 1–39.

Gu Z, Liu J, Yuan B *et al*., 1993. The changes of monsoon in the Qinghai-Tibet Plateau in the past 12000 years: Evidence of the geochemistry of Selincuo deposits. *Chinese Science Bulletin*, 38(1): 61–64. (in Chinese)

Hartmann K, Wünnemann B, 2009. Hydrological changes and Holocene climate variations in NW China, inferred from lake sediments of Juyanze palaeolake by factor analyses. *Quaternary International*, 194(1/2): 28–44.

Hastenrath S, 2007. Circulation mechanisms of climate anomalies in East Africa and the equatorial Indian Ocean. *Dynamics of Atmospheres and Oceans*, 43(1/2): 25–35.

Herzschuh U, 2006. Palaeo-moisture evolution in monsoonal Central Asia during the last 50,000 years. *Quaternary Science Reviews*, 25(1/2): 163–178.

Herzschuh U, Tarasov P, Wünnemann B *et al*., 2004. Holocene vegetation and climate of the Alashan Plateau, NW China, reconstructed from pollen data. *Palaeogeography*, *Palaeoclimatology*, *Palaeoecology*, 211(1/2): 1–17.

Hodell D A, Brenner M, Kanfoush S L *et al*., 1999. Paleoclimate of southwestern China for the past 50,000 yr inferred from lake sediment records. *Quaternary Research*, 52(3): 369–380.

Hong Y T, Hong B, Lin Q H *et al*., 2003. Correlation between Indian Ocean summer monsoon and North Atlantic climate during the Holocene. *Earth and Planetary Science Letters*, 211(3/4): 371–380.

Huang W, Chen J, Zhang X *et al*., 2015. Definition of the core zone of the "westerlies-dominated climatic regime", and its controlling factors during the instrumental period. *Science China Earth Sciences*, 58(5): 676–684.

Ji J F, Shen J, Balsam W *et al*., 2005a. Asian monsoon oscillations in the northeastern Qinghai-Tibet Plateau since the late glacial as interpreted from visible reflectance of Qinghai Lake sediments. *Earth and Planetary Science Letters*, 233(1/2): 61–70.

Ji S, Yang L Y, Yang X D *et al*., 2005b. Lake sediment records on climate change and human activities since the Holocene in Erhai catchment, Yunnan Province, China. *Science in China Series D-Earth Sciences*, 48(3): 353–363.

Jin M, Li G, Li F *et al*., 2015. Holocene shorelines and lake evolution in Juyanze Basin, southern Mongolian Plateau, revealed by luminescence dating. *The Holocene*, 25(12): 1898–1911.

Lau K M, Kim K M, Yang S, 2000. Dynamical and boundary forcing characteristics of regional components of the Asian summer monsoon. *Journal of Climate*, 13(14): 2461–2482.

Lennard C, Hegerl G, 2014. Relating changes in synoptic circulation to the surface rainfall response using self-organising maps. *Climate Dynamics*, 44(3/4): 861–879.

Leuschner D C, Sirocko F, 2003. Orbital insolation forcing of the Indian monsoon: A motor for global climate changes? *Palaeogeography*, *Palaeoclimatology*, *Palaeoecology*, 197(1/2): 83–95.

Li C Y, Wang Q, Liu X Y *et al*., 1982. Tectonic Map of Asia (scale 1:8000000). Beijing: Cartographic Publishing House.

Li J, Zeng Q, 2002. A unified monsoon index. *Geophysical Research Letters*, 29(8): 115-111–115-114.

Li Y U, Wang N A, Cheng H *et al*., 2008. Holocene environmental change in the marginal area of the Asian monsoon: A record from Zhuye Lake, NW China. *Boreas*, 38(2): 349–361.

Li Z, Wang N A, Cheng H *et al*., 2015a. Formation and environmental significance of late Quaternary calcareous root tubes in the deserts of the Alashan Plateau, Northwest China. *Quaternary International*, 372: 167–174.

Li Z, Wang N A, Li R *et al*., 2015b. Indication of millennial-scale moisture changes by the temporal distribution of Holocene calcareous root tubes in the deserts of the Alashan Plateau, Northwest China. *Palaeogeography*, *Palaeoclimatology*, *Palaeoecology*, 440: 496–505.

Liang X Z, Wang W C, 1998. Associations between China monsoon rainfall and tropospheric jets. *Quarterly Journal of the Royal Meteorological Society*, 124(552): 2597–2623.

Liu C, Wang H, Jiang D, 2004. The configurable relationships between summer monsoon and precipitation over East Asia. *Chinese Journal of Atmospheric Sciences*, 28(5): 700–712. (in Chinese)

Liu X, Shen J, Wang S *et al*., 2007. Southwest monsoon changes indicated by oxygen isotope of ostracode shells from sediments in Qinghai Lake since the late Glacial. *Chinese Science Bulletin*, 52(4): 539–544. (in Chinese)

Long A, 2001. Mid-Holocene sea-level change and coastal evolution. *Progress in Physical Geography*, 25(3): 399–408.

Long H, Lai Z, Fuchs M *et al*., 2012. Timing of Late Quaternary palaeolake evolution in Tengger Desert of northern China and its possible forcing mechanisms. *Global and Planetary Change*, 92/93: 119–129.

Long H, Lai Z, Wang N *et al*., 2010. Holocene climate variations from Zhuyeze terminal lake records in East Asian monsoon margin in arid northern China. *Quaternary Research*, 74(1): 46–56.

Lu R, 2001. Interannual variability of the summertime North Pacific subtropical high and its relation to atmospheric convection over the warm pool. *Journal of the Meteorological Society of Japan*, 79(3): 771–783.

Lu R Y, 2004. Associations among the components of the East Asian summer monsoon system in the meridional direction. *Journal of the Meteorological Society of Japan*, 82(1): 155–165.

Ma C, Zhu C, Zheng C *et al*., 2008. High-resolution geochemistry records of climate changes since late-glacial from Dajiuhu peat in Shennongjia Mountains, Central China. *Chinese Science Bulletin*, 53: 28–41.

Morrill C, Overpeck J T, Cole J E *et al*., 2006. Holocene variations in the Asian monsoon inferred from the geochemistry of lake sediments in central Tibet. *Quaternary Research*, 65(2): 232–243.

Overpeck J, Anderson D, Trumbore S *et al*., 1996. The southwest Indian monsoon over the last 18000 years. *Climate Dynamics*, 12(3): 213–225.

Qian W, Lin X, Zhu Y *et al*., 2007. Climatic regime shift and decadal anomalous events in China. *Climatic Change*, 84(2): 167–189.

Qiang M, Chen F, Wang Z *et al*., 2010. Aeolian deposits at the southeastern margin of the Tengger Desert (China): Implications for surface wind strength in the Asian dust source area over the past 20,000 years. *Palaeogeography*, *Palaeoclimatology*, *Palaeoecology*, 286(1/2): 66–80.

Shi X, Yu K, Chen T, 2007. Progress in researches on sea level changes in the South China Sea since Mid-Holocene. *Marian Geology and Quaternary Geology*, 27(5): 121–132. (in Chinese)

Sun X, Du N, Chen Y *et al*., 1993. Holocene palynological records in Lake Selincuo, northern Xizang. *Acta Botanica Sinica*, 35: 943–950. (in Chinese)

Taylor K E, Stouffer R J, Meehl G A, 2012. An overview of CMIP5 and the experiment design. *Bulletin of the American Meteorological Society*, 93(4): 485–498.

Tian L, Yao T, MacClune K *et al*., 2007. Stable isotopic variations in west China: A consideration of moisture sources. *Journal of Geophysical Research-Atmospheres*, 112(D10).

Trenberth K E, 1991. Climate diagnostics from global analyses-conservation of mass in ECMWF analyses. *Journal of Climate*, 4(7): 707–722.

Wang L, Chen W, Huang G *et al*., 2017. Changes of the transitional climate zone in East Asia: Past and future. *Climate Dynamics*, 49(4): 1463–1477.

Wang N A, Li Z, Li Y *et al*., 2012. Younger Dryas event recorded by the mirabilite deposition in Huahai Lake, Hexi Corridor, NW China. *Quaternary International*, 250: 93–99.

Wang N A, Li Z, Li Y *et al*., 2013. Millennial-scale environmental changes in the Asian monsoon margin during the Holocene, implicated by the lake evolution of Huahai Lake in the Hexi Corridor of Northwest China. *Quaternary International*, 313/314: 100–109.

Wang W, Feng Z, 2013. Holocene moisture evolution across the Mongolian Plateau and its surrounding areas: A synthesis of climatic records. *Earth-Science Reviews*, 122: 38–57.

Wu Y, Zheng X, Zhou L, 2012. The asynchronous nature of Holocene climate variability in China and its linkage to Asian monsoon and the westerly. *Research of Soil and Water Conservation*, 19(1): 27–32. (in Chinese)

Xiao J L, Xu Q H, Nakamura T *et al*., 2004. Holocene vegetation variation in the Daihai Lake region of north-central China: A direct indication of the Asian monsoon climatic history. *Quaternary Science Reviews*, 23(14/15): 1669–1679.

Yang X, Liu T, Xiao H, 2003. Evolution of megadunes and lakes in the Badain Jaran Desert, Inner Mongolia, China during the last 31,000 years. *Quaternary International*, 104(1): 99–112.

Yang X, Ma N, Dong J *et al*., 2010. Recharge to the inter-dune lakes and Holocene climatic changes in the Badain Jaran Desert, western China. *Quaternary Research*, 73(1): 10–19.

Yang X, Williams M A J, 2003. The ion chemistry of lakes and late Holocene desiccation in the Badain Jaran Desert, Inner Mongolia, China. *Catena*, 51: 45–60.

Yuan W, Yang Z, 2015. The Alashan Terrane did not amalgamate with North China block by the Late Permian: Evidence from Carboniferous and Permian paleomagnetic results. *Journal of Asian Earth Sciences*, 104: 145–159.

Zhang H C, Ma Y Z, Li J J *et al*., 2001. Palaeolake evolution and abrupt climate changes during Last Glacial Period in NW China. *Geophysical Research Letters*, 28(16): 3203–3206.

Zhang H C, Peng J L, Ma Y Z *et al*., 2004. Late Quaternary palaeolake levels in Tengger Desert, NW China. *Palaeogeography*, *Palaeoclimatology*, *Palaeoecology*, 211(1/2): 45–58.

Zhang S W, Yang Z Y, Cioppa M T *et al*., 2018. A high-resolution Holocene record of the East Asian summer monsoon variability in sediments from Mountain Ganhai Lake, North China. *Palaeogeography*, *Palaeoclimatology*, *Palaeoecology*, 508: 17–34.

Zhang X J, Jin L Y, 2016. Association of the Northern Hemisphere circumglobal teleconnection with the Asian summer monsoon during the Holocene in a transient simulation. *The Holocene*, 2015, 1–12.

Zhao H, Li G, Sheng Y *et al*., 2012. Early–middle Holocene lake-desert evolution in northern Ulan Buh Desert, China. *Palaeogeography*, *Palaeoclimatology*, *Palaeoecology*, 331/332: 31–38.

Zhao Y, Yu Z, Chen F *et al*., 2008. Holocene vegetation and climate change from a lake sediment record in the Tengger Sandy Desert, northwest China. *Journal of Arid Environments*, 72(11): 2054–2064.

Zheng Q, Zhang H, Ming Q *et al*., 2014. Vegetation and environmental changes since 15 ka B.P. recorded by lake Lugu in the Southwest Monsoon Domain Region. *Quaternary Sciences*, 34(6): 1314–1326. (in Chinese)

Zhong W, Xue J, Zheng Y *et al*., 2010. Climatic changes since the last deglaciation inferred from a lacustrine sedimentary sequence in the eastern Nanling Mountains, South China. *Journal of Quaternary Science*, 25(6): 975–984.

Zhu Q, He J, Wang P, 1986. A study of circulation differences between East-Asian and Indian summer monsoons with their interaction. *Advances in Atmospheric Sciences*, 44(4): 466–477.

Zhu Z, Wu Z, Liu S *et al*., 1980. Introduction to the Desert in China. Beijing: Science Press. (in Chinese)

Ziv B, Dayan U, Kushnir Y *et al*., 2006. Regional and global atmospheric patterns governing rainfall in the southern Levant. *International Journal of Climatology*, 26(1): 55–73.